Degradation of Lindane using two nanosized BiOXs and their heterojunction under visible light

Tarek S. Jamil*, Eman S. Mansor, Rabab A. Nasr

Water Pollution Control Department, National Research Center, Cairo, Egypt, Tel. +2 012 848 777 31;
email: Omaytarek73@yahoo.com (T.S. Jamil), Tel. +2 012 5210459; email: eman_mansor31@yahoo.com (E.S. Mansor),
Tel. +2 01006210880; email: rababelsheikh@yahoo.com (R.A. Nasr)

ABSTRACT

In this paper, bismuth oxybromide (BiOBr), bismuth oxyiodide (BiOI), and heterojunction ($BiOI_{0.5}Br_{0.5}$) were prepared via facile co-precipitation method, a low-temperature solution route, and facile chemical etching method, respectively. They were prepared by Bi $(NO_3)_3\cdot5H_2O$ as the Bi source. The resulting BiOBr, BiOI, and $BiOI_{0.5}Br_{0.5}$ photocatalysts were fully characterized using X-ray diffraction, energy-dispersive X-ray spectroscopic, scanning electron microscopy, high-resolution transmission electron microscopy, SAED, Brunauer–Emmett–Teller surface area, and UV–vis diffuse reflectance spectra techniques. The prepared photocatalysts were of pure tetragonal phase, and homogeneous particles. Their surface area are 6.19, 296.6, and 186.6 m^2/g, and their band gaps were about 2.9, 1.9, and 2.1 eV for BiOBr, BiOI, and $BiOI_{0.5}$ $Br_{0.5}$, respectively. Their photocatalytic property was investigated by the degradation of Lindane in aqueous solution under commercial visible metal halide lamp. The optimum amounts of BiOBr, BiOI, and $BiOI_{0.5}Br_{0.5}$ powders were 1.0 g/L at pH 8 that degraded 60, 80, and 95% of Lindane, respectively, after 2 h of irradiation. Moreover, $BiOI_{0.5}Br_{0.5}$ heterojunction exhibited much higher photocatalytic activity for the degradation of Lindane under visible light ($\lambda > 420$ nm) than pure BiOBr and BiOI, Since, the reaction kinetic constants for degradation of Lindane by BiOBr, BiOI, and $BiOI_{0.5}Br_{0.5}$ heterojunction were 0.0073, 0.0126, and 0.0194 min^{-1}, respectively. It is a prospective strategy for constructing highly efficient bismuth halide-based heterojunction to eliminate organic pollutants in water.

Keywords: Visible light; Degradation; BiOX; Lindane

1. Introduction

Lindane is an organochlorine pesticide (OCP) and a persistent organic pollutant which has been used as an insecticide on fruit, vegetables, and forest crops on a wide range of soil-dwelling and plant-eating insects [1]. It has been found in groundwater samples, as well as in the marine environment. Due to its high toxicity, it is classified as restricted use pesticide, purchased only to certify applicators [2]. It is classified by the USEPA and World Health Organization as "Moderately Hazardous," and it may be a carcinogen and a teratogen. Its low aqueous solubility, relative high stability, lypophilicity, and chlorinated nature

*Corresponding author.

contribute to its environmental persistence and resistance to degradation [3].

Among these contaminants, OCPs are one of the largest groups of pollutants such as Lindane residues in river, soil, and groundwater [4]. Also they are most persistent pesticides in the environment. Although application of some chloro-organic insecticides in agriculture was banned in most countries in the last 20 years, thousands of tons of obsolete pesticide deposits in farms and tombs jeopardize the environment.

Semiconductor-assisted photocatalysis has been found in supplementary and complementary to conventional approaches aimed at destruction or transformation of hazardous chemical waste such as high temperature incineration, activated sludge digestion, anaerobic digestion, and physico-chemical treatment [4]. Heterogeneous photocatalytic oxidation using titanium dioxide (TiO_2) as a photocatalyst has a great attention for several years in oxidation of a variety of organic and inorganic compounds [5].

Recently, bismuth oxyhalides BiOX and BiOX/ BiOY (X, Y = Cl, Br, I) heterojunction have been utilized because of their unique properties and potential applications. Bismuth oxyhalides have different band gap energies as shown in Table 1 [6].

Accordingly, BiOI and BiOBr are relatively stable under visible light absorption. In addition, their matching band structures are conducive to the construction of heterojunction between BiOI and BiOBr that enhances the photocatalytic activities of BiOX [7,8]. Recently, the role of heterostructures in enhancing the photocatalytic performance has attracted much attention since it exhibits high separation efficiency of photogenerated electrons and holes, which effectively protects the semiconductor to avoid its photoreduction and gives rise to high activity and stability in degradation of the typical water pollutants [9]. Currently, many novel heterostructures, with the aim to amend the drawbacks of common semiconductors, have been used such as $CdS/BiPO_4$ [10], Ag_2O/ Ag_2CO_3 [9], Ag_2O nanowire network/TiO_2 nanotube [11], and growth of BiOBr nanosheets on C_3N_4 nanosheets to construct two-dimensional nanojunctions with enhanced photo reactivity [12]. Also, several BiOI-based heterojunctions can be used as

photocatalyst such as $BiOI/TiO_2$ [13], BiOI/ZnO [14], BiOI/AgI [15], $BiOI/Bi_2O_3$ [16], BiOI/BiOBr [8], and BiOI/BiOCl [17]. BiOX heterojunction are widely applicable photocatalysts and used for different environmental applications like wastewater treatment, air pollution control, and splitting of water; but the majority of research studies focus on the utilization of BiOX for water treatment processes. Since, BiOX is capable to degrade a plethora of different pollutants [18]. BiOX has been applied for the degradation of different types of dyes such as Rhodamine B [19], methyl orange [20], methylene blue [21], and Azure B [22]. The results have demonstrated that they can be effectively reduced to non-toxic products by visible light photocatalysis using BiOX. Also, BiOX are widely used for degradation of organic in water such as BPA, benzotriazole, toluene, and polybrominated diphenyl ethers [23–27]. In addition to organics and organic dyes removal, BiOX systems have also been applied to systems containing micro-organisms to observe its effects on disinfection and bring about heavy metal reduction in wastewater such as chromium(VI) [28,29]. This opens up a lot of possibilities for application of BiOX photocatalysis systems under UV and visible light irradiation.

It is generally known that the noble metal/ semiconductor oxide heterojunction system could reduce the electron/hole recombination rate due to better charge separation. Accordingly, noble metal deposition can be used to improve the photocatalytic performance of BiOX [30]. More recently, the deposition of Ag nanoparticles (NPs) on BiOX has been found to give a surprising efficiency in decomposition of dyes under UV or visible light irradiation [31,32]. Also, a series of novel noble metal (Rh, Pd, Pt) deposited BiOX photocatalysts are found to have enhanced photocatalytic performance in dye degradation [30].

The aim of this manuscript is testing of the preparation of microsphere BiOBr, BiOI nanoplates, and $BiOI_{0.5}Br_{0.5}$ via different methods and their characterization by several instruments. Finally, their photocatalytic activities were studied through Lindane removal in aqueous solution under visible light.

2. Materials and methods

2.1. Material

Lindane of purity 99%, were purchased from Sigma Aldrich Company and were used without further purification. All reagents used for preparation of BiOX and $BiOI_{0.5}Br_{0.5}$ heterojunction, pH adjustment, and washing of the prepared photocatalyst were submitted by Merck Company.

Table 1
Band gap energies for bismuth oxyhalides (BiOX)

BiOX	Band gap energy
BiOCl	3.19–3.44
BiOBr	2.64–2.91
BiOI	1.77–1.92

2.2. Preparation of photocatalysts

Sphere BiOBr was synthesized via facile co-precipitation method by dissolving 0.05 mol $Bi(NO_3)_3 \cdot 5H_2O$ in 0.5 M 100 mL NaBr solution. The resulting suspension was magnetically stirred for 24 h at room temperature. The obtained precipitates were collected and rinsed with de-ionized water and absolute ethanol several times, and dried at 60°C for 6 h [26]. While, BiOI plates were prepared via a low-temperature solution route by addition of 0.05 mol of $Bi(NO_3)_3 \cdot 5H_2O$ to 450 mL of distilled water under magnetic stirring for 30 min. Then, 0.5 M of 100 mL KI was added drop wisely into the white suspend solution, and the mixture was heated at 80°C for 5 h in water bath. Finally, the resulting precipitates were collected and washed with deionized water and ethanol then dried at 60°C in air for 4 h [33].

On the other hand, $BiOI_{0.5}Br_{0.5}$ heterojunction was prepared by dispersing 2.00 g of previously prepared BiOBr into 400 mL deionized water adjusted to pH 2.65 by glacial acetic acid with constant stirring. Then, a stoiciometric amount of KI was added drop wise into the suspension solution of BiOBr. The mixture was stirred for 30 min at room temperature. Finally, the brick red $BiOI_{0.5}Br_{0.5}$ precipitates with molar weight % in [I/(I + Br)] ratio 50% were collected, washed, and dried at 80°C for 3 h [34].

2.3. Characterization of the prepared photocatalyst

The prepared photocatalyst powders were characterized by X-ray diffraction (XRD) using Philips powder diffractometer. While, energy-dispersive X-ray spectroscopic (EDX) measurements were performed using an Oxford instruments INCA X-sight. The morphology was determined by scanning electron microscopy (SEM, XT810, inspect S) and JEOL JEM-2100 high-resolution transmission Electron microscopy (HRTEM). UV–vis diffuse reflectance spectra (DRS) were obtained using a UV–vis spectrophotometer (JASCO V-570). While, The Brunauer–Emmett–Teller (BET) surface area was determined by using apparatus NOVA Surface Area Analyzer from Quantachrome Instruments.

2.4. Experimental set-up

The photocatalytic degradation reaction was carried out using a slurry-mode batch reactor equipped with a cooling jacket (Fig. 1) with continuous stirring. The source of visible light was carried out by commercial visible metal halide lamp (HQI-T 250/Daylight, OSRAM GmbH, Germany) with lumi-
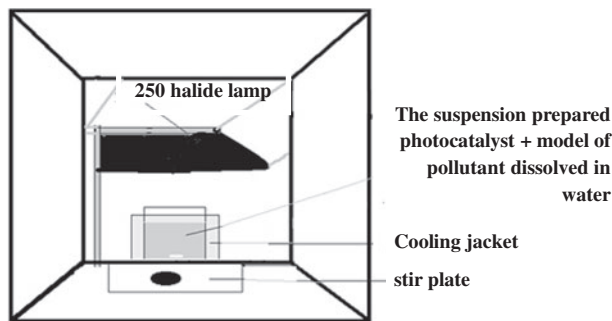
Fig. 1. Experimental set up of visible light photocatalytic reactor.

nous flux of irradiation 20,000 lm with luminous efficacy of 82 lm/W. About 5 ml sample was taken from the reaction suspension at given time intervals and photocatalyst was separated from the solution by centrifugation. The entire setup was placed in a reflective housing in order to prevent external light from entering the system as well as keep the light generated by the lamp within the setup.

2.5. Analysis

The concentrations of Lindane was monitored with HP 6890 Gas Chromatography using Electron Capture Detector by HP-19091A ultra1 methyl Siloxane capillary column (30 m × 0.2 mm ID, 0.33 μm film thickness) according to EPA method 508 Rev. 3 [35] using liquid–liquid extraction according to USEPA Method 608 [36].

3. Results and discussion

3.1. Characterization

The phase purity and crystallographic structure of the prepared BiOBr, BiOI, and $BiOI_{0.5}Br_{0.5}$ photocatalysts were examined using powder XRD measurements. Fig. 2 shows the XRD patterns of the prepared photocatalysts. All the detectable peaks in the pattern were pure tetragonal phase BiOBr, BiOI, and $BiOI_{0.5}Br_{0.5}$ which are in good agreement with the literature values (JCPDS file Card No. 09-0393 and No. 10-0445) respectively.

No characteristic peaks of other compounds are detected, showing high purity of the product. The peaks are narrow and intense which implies good crystallinity of BiOBr, BiOI, and $BiOI_{0.5}Br_{0.5}$ photocatalysts; the wide peaks imply small crystalline size of the products.
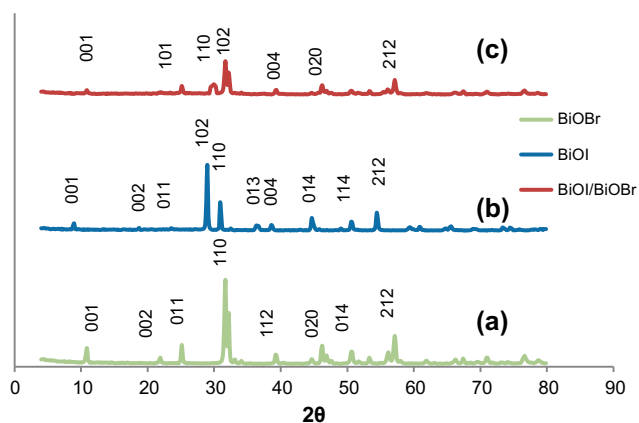
Fig. 2. XRD patterns of (a) BiOBr, (b) BiOI and (c) BiOI/BiOBr heterojunction.

Additional evidence of the formation of the as-prepared photocatalysts came from EDS (Fig. 3) that shows BiOX are composed of only Bi, O, and halide atoms [37]. In case of $BiOI_{0.5}Br_{0.5}$ heterojunction, the atomic ratio of $[I/(I + Br)]$ was provided as 0.5 (Fig. 3(c)) which basically confirms the previous stoichiometric preparation as well as XRD analysis.

The microstructure and the morphology of the products were investigated by SEM as shown in (Fig. 4). For BiOBr, SEM images of the synthesized BiOBr catalysts had a non-regular microsphere shape (Fig. 4(b)) [26] and at high magnification SEM image of an individual non-regular microsphere shows that the as-prepared product is constructed of many nanosheets (Fig. 4(a)). While, SEM image of BiOI shows that it is consisted of irregular nanoplates (Fig. 4(c)). On the other hand, SEM images of $BiOI_{0.5}Br_{0.5}$ (Fig. 4(d)) shows that the heterojunction is composed of irregular nanoplates, microsphere with smooth surfaces which is confirmed by HRTEM images (Fig. 5).

As the photo absorption and the microstructure of semiconductors strongly affect solar energy conversion and photocatalytic degradation processes, so UV–vis diffuse reflectance spectra analysis of the powders were performed. The UV–vis absorption edges of BiOX powders have a clear red shift with increasing X atomic numbers in sequence [38], The BiOBr powders have intense absorption edges at about 440 nm in the visible light regions. While BiOI/BiOBr powders have obvious absorption edges at about 645 nm in the visible light region and BiOI powders have obvious absorption edges at about 700 nm in the visible light region as shown in Fig. 6.

It is important to study the optical absorption of the as prepared photocatalysts before the photocat-

alytic activity characterization because the UV–vis absorption edge is relevant to the band gap of semiconductor catalyst. The diffuse reflectance data are used to calculate the absorption coefficient from the Kubelka–Munk (KM) [39] function (Eq. (1)) defined as:

$$F(R_\infty) = \alpha/S = (1 - R_\infty)^2/R_\infty \tag{1}$$

where α, S, and $F(R_\infty)$ is the absorption coefficient, scattering coefficient, and KM function, respectively. As a crystalline semiconductor, it is well known that the optical absorption near the band edge follows the formula (Eq. (2)):

$$\alpha E = C(E - E_g)^n \tag{2}$$

where α, E, E_g, and C is the absorption coefficient, incident photon energy, the band gap energy and a constant, respectively.

The band gap energies E_g for the prepared photocatalysts were measured as shown in Fig. 6 (the insert). Since, the intercept on abscissa of the line by plotting $(F(R_\infty)E)^{1/2}$ vs. photoenergy give the values of band gap energy (E_g) [28]. The E_g estimated from the intercept of the tangents to the plots were 2.9, 1.9, and 2.1 eV BiOBr, BiOI, and $BiOI_{0.5}Br_{0.5}$ samples, respectively.

The specific surface area and porosity of the prepared photocatalysts were measured from the nitrogen adsorption analysis. The prepared photocatalysts exhibit type-IV isotherms (Fig. 7) that is typical to mesoporous solids.

The BET-specific surface areas (A_{BET}) of BiOBr, BiOI, and $BiOI_{0.5}Br_{0.5}$ were calculated to be 6.19, 296.6, and 186.6 m^2/g, respectively. The obtained results show that the A_{BET} of all the prepared photocatalysts have obvious difference, which implies that A_{BET} will have significant effect on the photocatalytic performance of different photocatalysts. The surface area of the prepared BiOI and $BiOI_{0.5}Br_{0.5}$ used in this study is very high compared with literature either prepared by the same method [34] or by different methods [38].

3.2. Photocatalytic degradation

Fig. 8 shows the effect of irradiation time on the photocatalytic degradation of Lindane using the different prepared photocatalysts at pH 6.8, initial dose of catalyst 0.75 g/L, and Lindane concentration 8 ppm. It is obvious that the degradation efficiency of Lindane increased with the increase of irradiation time. At
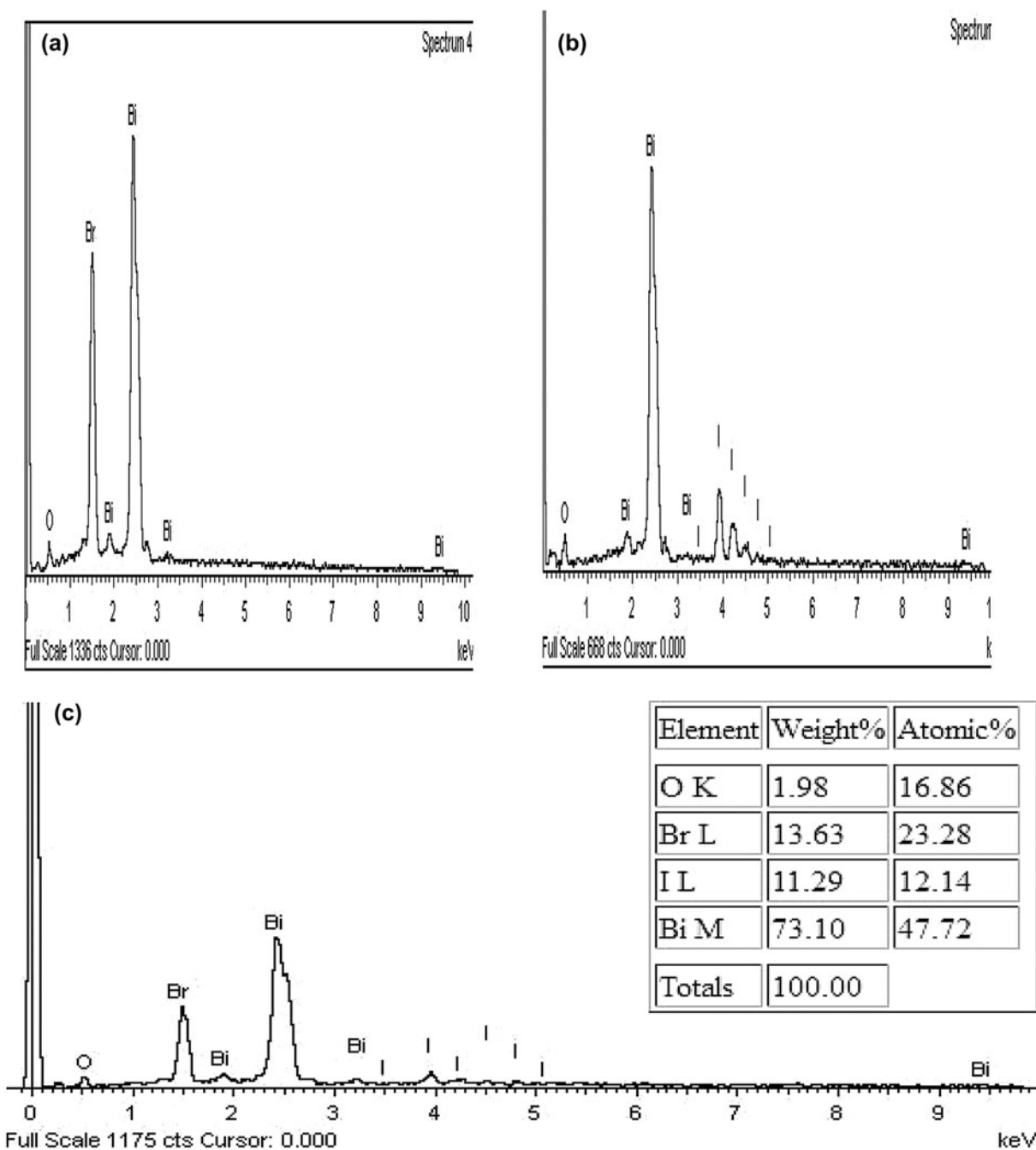
Fig. 3. EDS spectrum of (a) BiOBr, (b) BiOI and (c) BiOI/BiOBr hetrojunction with its elemental analysis.

120-min irradiation time, the percent removal reached 36, 53, and 64% for BiOBr, BiOI, and $BiOI_{0.5}Br_{0.5}$, respectively. With more increase of irradiation time, non-significant increase in removal was observed. Accordingly, the optimum irradiation time for the degradation of Lindane is 120 min.

The catalyst loading for the photocatalytic degradation process is an important parameter as it determines the amount of catalyst expended per cycle and therefore the optimum loading must be determined.

It can be noticed in Fig. 9 that as catalyst dosage is increased from 0.25 g/L, the activity also increases up to a catalyst dosage of 1.0 g/L then it decrease at catalyst dosage 1.25 g/L. So, maximum removal was observed at 1.0 g/L catalyst dose of BiOBr, BiOI, and $BiOI_{0.5}Br_{0.5}$ with irradiation time of 120 min. This
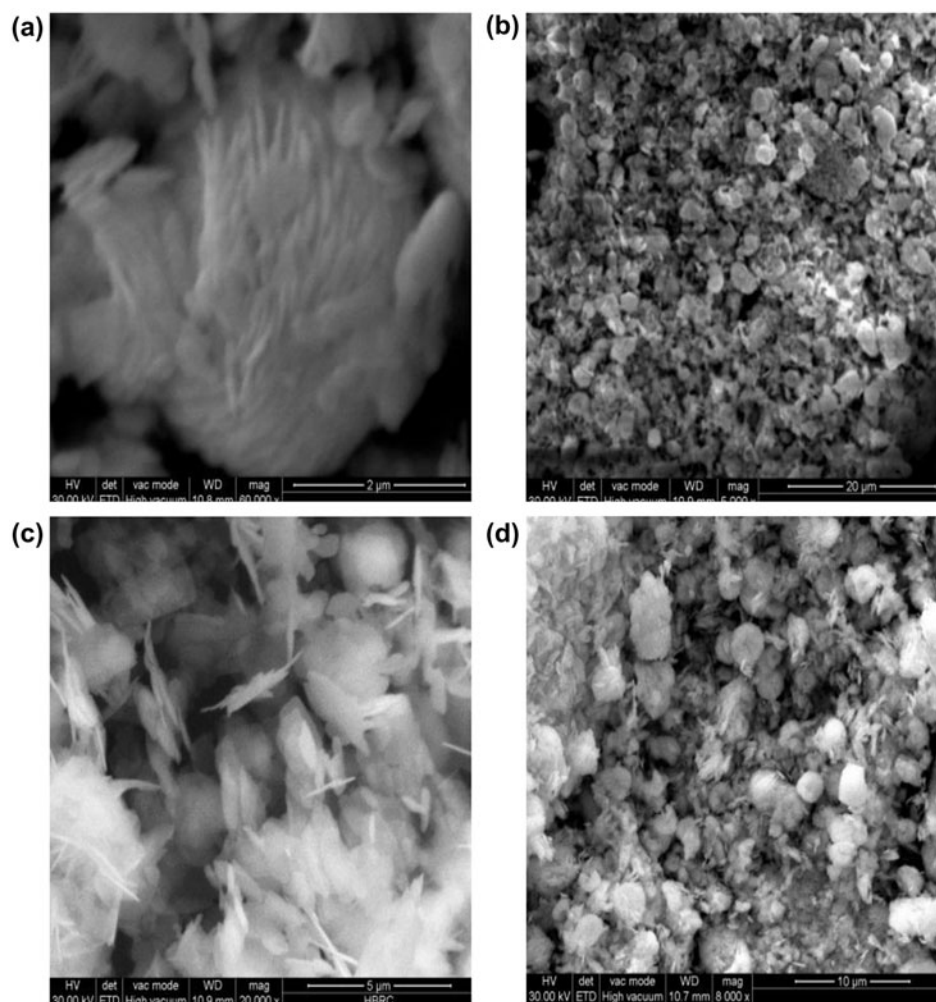
Fig. 4. Typical SEM images of the prepared photocatalysts (a and b) BiOBr (c) BiOI, and (d) BiOI/BiOBr.
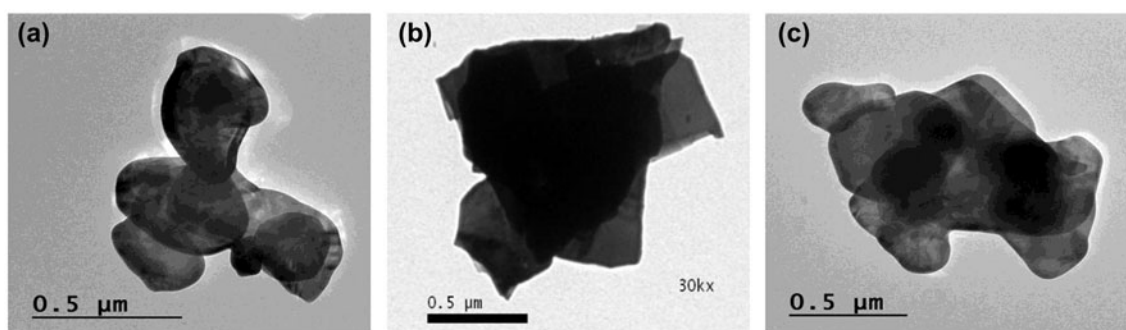
Fig. 5. HRTEM images of the prepared photocatalysts (a) BiOBr, (b) BiOI and (c) BiOI/BiOBr.

can be attributed to increase in the number of available active sites by increasing catalyst loading that leads to increases the electron/hole pairs so increases the amount of hydroxyl radicals produced, thus the photocatalytic activity is enhanced [40,41].
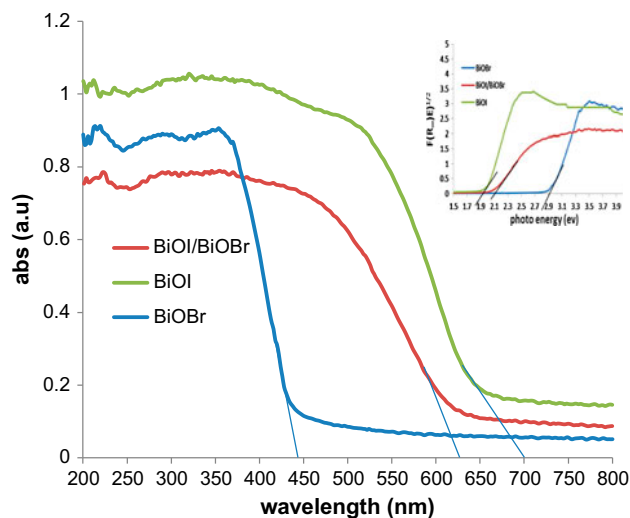
Fig. 6. UV–vis DRS of the prepared photocatalyst. Insert: relation between $F(R_\infty)E)^{1/2}$ vs. photo energy.
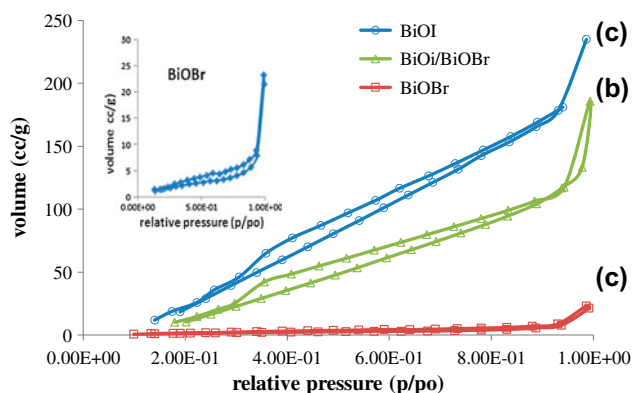
Fig. 7. N$_2$ adsorption and desorption isotherms for the prepared photocatalysts (a) for the BiOBr microspheres, (b) the heterojunction of BiOI/BiOBr and (c) for the BiOI nanoplates.

However, increasing the catalyst loading (at 1.25, g/L catalyst dose) excessively affects negatively the photocatalytic activity due to higher extent of light scattering which negatively impacts light penetration [42–44]. As a result, the photoactivity is reduced and a dosage of 1.0 g/L is deemed as the optimized dosage.

The pH value of the solution is an important factor influencing the degradation of model pollutant in the photocatalytic process and can also be a critical operational variable [45–47]. Altering the initial pH can vary electrostatic interaction between the reactant and the prepared photocatalysts surface and also shift the potential of redox reaction affecting the adsorption and reactivity of organic solutes [48,49]. The effects of
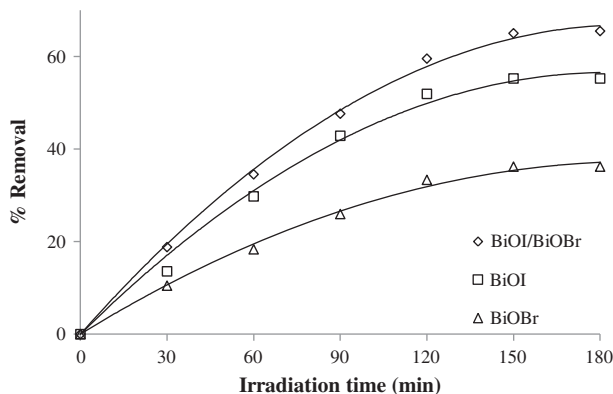
Fig. 8. % Removal as a function of irradiation time on the photocatalytic degradation of Lindane (pH 6.5, dose of catalyst 0.75 g/L, Lindane concentration 8 ppm).

pH on photo degradation performance of the prepared photocatalysts were therefore evaluated.

The initial pH of 8 ppm Lindane without any adjustment was found to be 6.8 in the deionized water solution. The effect of pH on degradation of Lindane by the prepared photocatalysts is presented in Fig. 10. When the pH is decreased below the natural pH, the degradation rate is lower, However, as the pH is increased, the degradation rate increases, reaching a maximum at around pH 8. However, the degradation activity of Lindane decreases gradually when the pH exceeds 8. The results can be explained by the recognized effects of pH on surface charge of catalyst and pollutants, absorption of contaminants on surface of the photocatalyst, and hydroxyl concentration, which ultimately affect the degradation efficiency [50]. For an amphoteric material such as BiOX, the change in the concentrations of H$^+$ and OH$^-$ can affect its net surface charges.

When the solution pH is lower than 4.0, both the catalyst and pollutants are positively charged. As a result, the degradation of Lindane on the BiOBr, BiOI, and BiOI$_{0.5}$Br$_{0.5}$ surface is lower and this leads to lower degradation at lower pH values.

Apparently, the increasing degradation rate with pH 8 could be attributed to the fact that in alkaline media, a higher level of hydroxide ions (OH$^-$) induced the generation of hydroxyl-free radicals (OH·) as shown in Eqs. (3)–(8). The formation of hydroxyl-free radicals occurs from photo-oxidation of OH$^-$ by holes forming on the surface of the BiOX photocatalysts [51]. Since hydroxyl-free radicals are the primary oxidizing species in degradation of Lindane, the rate of degradation is increased as the pH of the solution is increased. However, as the pH is increased beyond the ideal point degradation is decrease, this is because
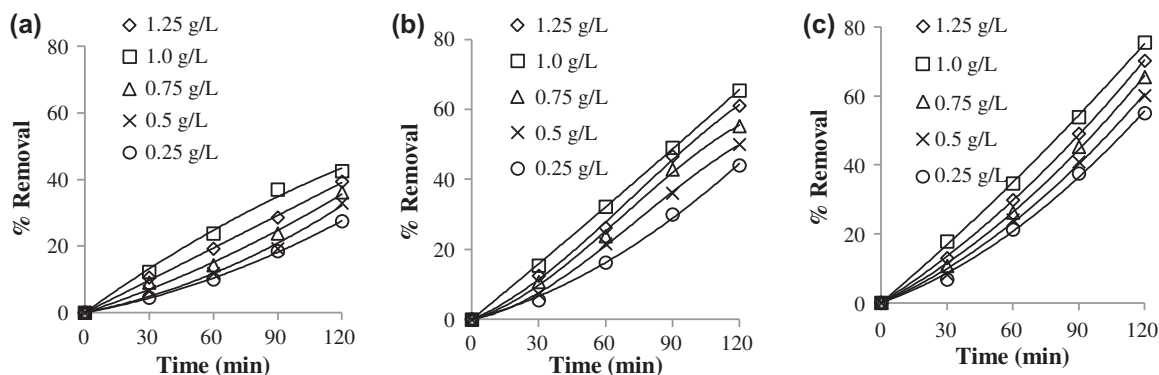
Fig. 9. % Removal of Lindane under visible light irradiation using various (a) BiOBr doses, (b) BiOI and (c) BiOI/BiOBr.
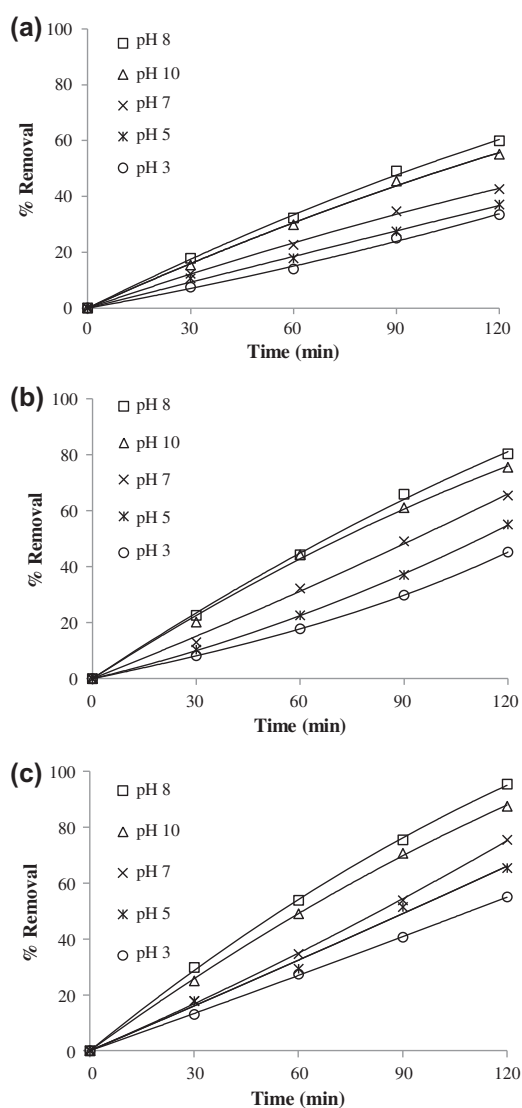
Fig. 10. % Removal of Lindane under visible light irradiation using (a) BiOBr, (b) BiOI and (c) BiOI/BiOBr at different pH values.

the pollutant and BiOX molecules at higher pH repel, lowering the absorption of Lindane on the surface of photocatalyst, which is known to lead to poor photochemical degradation [24].

$$\text{BiOX} + h\nu \ (\lambda < 400 \ \text{nm}) \rightarrow \text{BiOX} \ (e_{cb}^- + \ h_{vb}) \quad (3)$$

$$\text{BiOX} \ (e_{cb}^-) + O_2 \rightarrow \text{BiOX} + O_2^{\cdot-} \quad (4)$$

$$h^+ + \ H_2O \ \rightarrow \ OH^\cdot \quad (5)$$

$$e^- + \ O_2 \rightarrow O_2^{\cdot-} \rightarrow \ H_2O_2 \rightarrow 2OH^\cdot \quad (6)$$

$$h_{vb+} + \text{polluted} \ \rightarrow \text{degradation product} \quad (7)$$

$$O_2^{\cdot-} + \text{polluted} \ \rightarrow \ \text{degradation product} \quad (8)$$
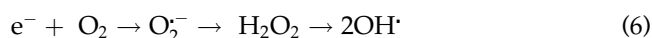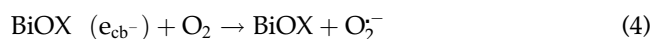
In order to establish the dependence of removal efficiency on the pollutant concentration, solutions of different initial concentrations of Lindane were degraded using the same photocatalysts and amount of photocatalyst, 1.0 g/L of each separately. The results shown in Fig. 11 indicate that the activity of the photocatalyst decreases with increasing Lindane concentration (2, 4, 6, 8 ppm). The relationship between pollutant concentration and photocatalytic activity is associated with the absorption of reactant on the surface of photocatalyst [52]. Therefore, increasing the pollutant concentration decreases activity due to the limitation of the number of active sites available for pollutant molecules on the photocatalyst surface [53]. Also with increasing pollutant concentration, more and more organic intermediates compete with hydroxyl ions for absorption at the active sites of photocatalysts, thus reducing the generation of hydroxyl radicals [54,55].
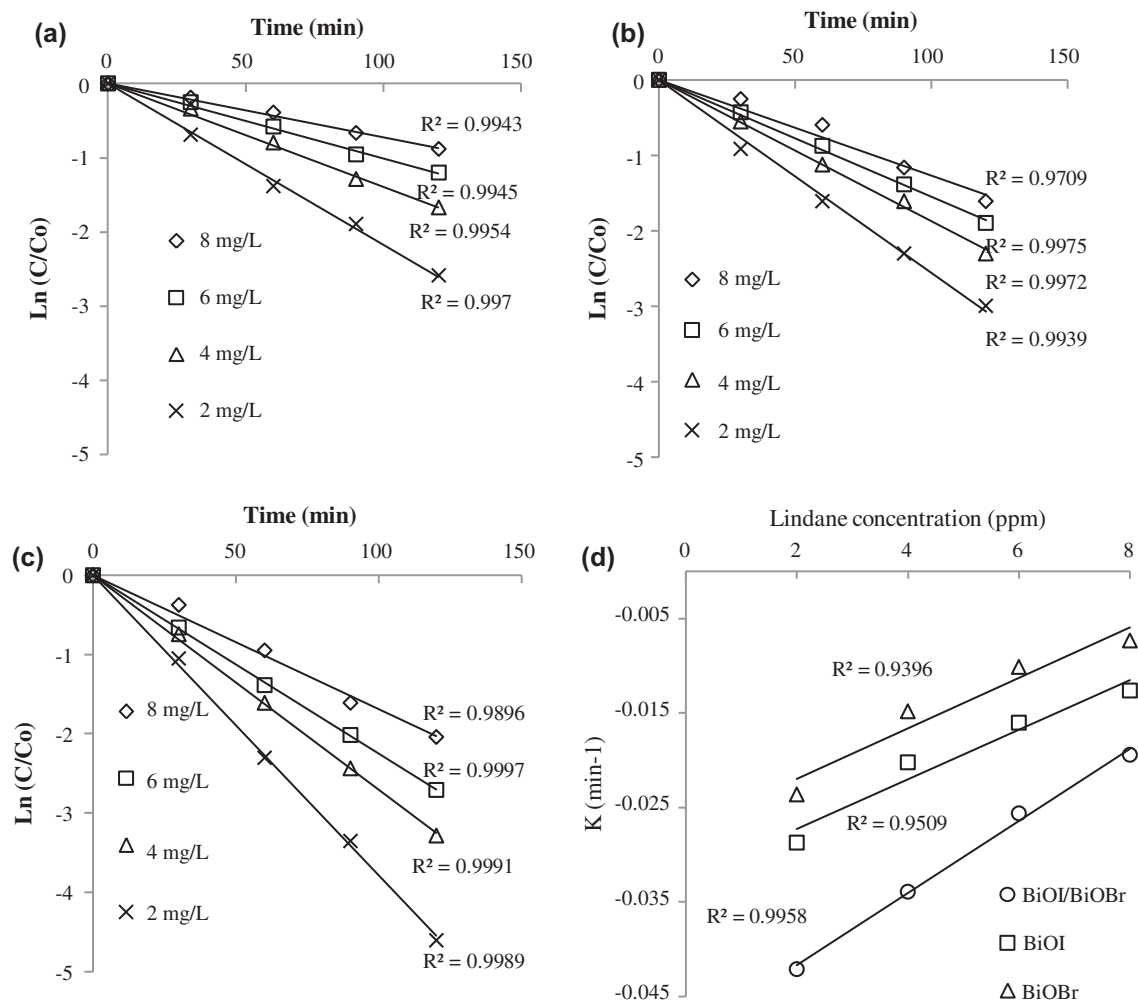
Fig. 11. Pseudo-first-order kinetic of Lindane (a) by BiOBr, (b) by BiOI, (c) by BiOI/BiOBr photocatalysts at Lindane different concentration and (d) degradation rate constant values for the prepared photocatalysts.

The heterogeneous mixture of Lindane with the prepared photocatalysts was separately exposed to visible radiation. The degradation rate arranged in the order $BiOI_{0.5}Br_{0.5} > BiOI > BiOBr$ using visible irradiation as shown in (Fig. 11(a)–(c)). Based on the linear relationship; the degradation of Lindane followed the pseudo-order kinetics which is represented by Eq. (9).

$$\ln\left(\frac{C}{C_o}\right) = K_{app}t \qquad (9)$$

where the observed rate constant, and C_o and C are the concentrations of phenol at $t = 0$ and t, respectively. For more clear understanding of the relationship between the reactivity and catalyst prepared, k_{app} was plotted vs. substrate concentrations as mentioned

in (Fig. 11(d)). The heterojunction $BiOI_{0.5}Br_{0.5}$ showed the highest removal at the optimum operating conditions followed by BiOI and BiOBr was the lowest. Therefore, it is very characteristic that the prepared photocatalysts showed a high visible light response.

The lower performance of BiOBr in Lindane degradation can be attributed to undesirable positions of conduction bands which hinder its performance for Lindane under visible light despite its merits of suitable band gap for visible light photocatalysis, layered structure and indirect semiconducting ability [56].

It is well known that photocatalytic activity is closely related to the size, morphology, and structure of photocatalysts. Nanoscale materials are believed to perform better than micro materials due to the larger surface area and the faster arrival to the reaction sites of the photogenerated electrons and holes [57]. In addition, band structure (Fig. 12) has an influence on
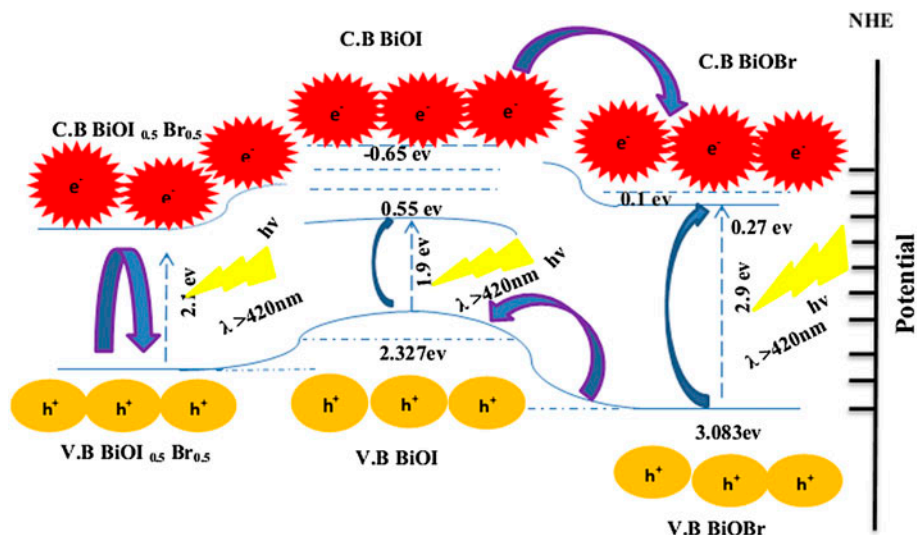
Fig. 12. Illustration of structural band gap for the prepared photocatalyst.

controlling the properties of photocatalysts. Apparently, the nested band edges of BiOBr (E_{VB} = 3.083 eV, E_{CB} = 0.27 eV), and BiOI (E_{VB} = 2.327 eV, E_{CB} = 0.55 eV) in single state are unfavorable for the separation of the photo-induced carriers. However, in the $BiOI_{0.5}Br_{0.5}$ heterojunction, the VB edge of BiOI could be rose up to a higher potential edge (−0.65 eV) under visible light with energy less than 2.9 eV (λ > 420 nm), while that of BiOBr is only up to 0.10 eV. Herein, the reformed band edges for the $BiOI_{0.5}Br_{0.5}$ heterojunction will become an more reactive structure. Under visible light irradiation, the electrons can be excited easily from the VB to the CB of BiOI and then injected into the more positive CB of BiOBr, followed by the reaction with O_2 adsorbed on the surface of $BiOI_{0.5}Br_{0.5}$ to produce $O_2^{\cdot-}$ and H_2O_2 that decompose organic pollutants [8,13,17,34,58]. On the contrary, the photogenerated holes left on the VB of BiOBr can transfer to the VB of BiOI, and then react directly with organic pollutants. Hence, the photo-generated electron-hole pairs are efficiently separated across the heterojunction interface formed between BiOI and BiOBr, which is mainly responsible for the enhanced photocatalytic activity of BiOI/BiOBr. So, these modifications lead directly to the enhancement of the absorption capacity of the photocatalyst [56]. Accordingly, the photocatalytic activity of $BiOI_{0.5}Br_{0.5}$ heterojunction is much higher than that of single BiOI and BiOBr.

4. Conclusion

In this study, two BiOX were and their $BiOI_{0.5}Br_{0.5}$ heterojunction were successfully prepared via facile different methods which are facile co-precipitation method (for BiOBr), a low-temperature solution route (BiOI), and facile chemical etching method (BiOI/ BiOBr), respectively. The prepared photocatalysts were fully characterized by different instruments since, BiOI and $BiOI_{0.5}Br_{0.5}$ heterojunction show very high-surface area and low-band gap energy compared with BiOBr. All obtained BiOX catalysts exhibited remarkable photocatalytic activities on Lindane under visible light irradiation, which may be due to their special structure and low band gap.

Hydroxyl radical $HO^{\cdot}$ and holes played an important role in the photodegradation of Lindane over the prepared photocatalysts. The results indicated that BiOI and heterojunction $BiOI_{0.5}Br_{0.5}$ catalysts might act as promising materials in the field of agriculture wastewater treatment by photocatalysis using low-cost visible light and its applications for agriculture reuse.

References

[1] A. Tor, M. Aydin, S. Aydin, M. Tabakci, F. Beduk, Removal of lindane from an aqueous solution by using aminopropyl silica gel-immobilized calix[6] arene, J. Hazard. Mater. 262 (2013) 656–663.

[2] S. Antonaraki, T.M. Triantis, E. Papaconstantinou, A. Hiskia, Photocatalytic degradation of lindane by polyoxometalates: Intermediates and mechanistic aspects, Catal. Today 151 (2010) 119–124.

[3] I. San Román, M.L. Alonso, L. Bartolomé, A. Galdames, E. Goiti, M. Ocejo, M. Moragues, R.M. Alonso, J.L. Vilas, Relevance study of bare and coated zero valent iron nanoparticles for lindane degradation from its by-product monitorization, J. Chemosphere 93 (2013) 1324–1332.

[4] J. Senthilnathan, L. Philip, Photocatalytic degradation of lindane under UV and visible light using N-doped TiO_2, Chem. Eng. J. 161 (2010) 83–92.

[5] J.M. Herrmann, Heterogeneous photocatalysis: state of the art and present applications In honor of Pr. R.L. Burwell Jr. (1912–2003), Former Head of Ipatieff Laboratories, Northwestern University, Evanston (Ill), Top. Catal. 34 (2005) 49–65.

[6] A. Ahmad, Synthesis and Evaluation of Photocatalytic Properties of BiOBr for Wastewater Treatment Applications, MSc thesis, 2013.

[7] X. Chang, M.A. Gondal, A.A. Al-Saadi, M.A. Ali, H. Shen, Q. Zhou, J. Zhang, Photodegradation of Rhodamine B over unexcited semiconductor compounds of BiOCl and BiOBr, J. Colloid Interface Sci. 377 (2012) 291–298.

[8] J. Cao, B. Xu, B. Luo, H. Lin, S. Chen, Novel BiOI/BiOBr heterojunction photocatalysts with enhanced visible light photocatalytic properties, Catal. Commun. 13 (2011) 63–68.

[9] C. Yu, G. Li, S. Kumar, K. Yang, R. Jin, Phase transformation synthesis of novel Ag_2O/Ag_2CO_3 heterostructures with high visible light efficiency in photocatalytic degradation of pollutants, Adv. Mater. 26 (2014) 892–898.

[10] D. Chen, Z. Kuang, Q. Zhu, Y. Du, H. Zhu, Synthesis and characterization of $CdS/BiPO_4$ heterojunction photocatalyst, Mater. Res. Bull. 66 (2015) 262–267.

[11] C. Liu, C. Cao, X. Luo, S. Luo, Ag-bridged Ag_2O nanowire network/TiO_2 nanotube array p–n heterojunction as a highly efficient and stable visible light photocatalyst, J. Hazard. Mater. 285 (2015) 319–324.

[12] Y. Sun, W. Zhang, T. Xiong, Z. Zhao, F. Dong, R. Wang, W.K. Ho, Growth of BiOBr nanosheets on C_3N_4 nanosheets to construct two-dimensional nanojunctions with enhanced photoreactivity for NO removal, J. Colloid Interface Sci. 418 (2014) 317–323.

[13] X. Zhang, L.Z. Zhang, T.F. Xie, D.J. Wang, Low-temperature synthesis and high visible-light-induced photocatalytic activity of $BiOI/TiO_2$ heterostructures, J. Phys. Chem. 113 (2009) 7371–7378.

[14] J. Jiang, X. Zhang, P. Sun, L. Zhang, ZnO/BiOI heterostructures: photo induced charge transfer property and enhanced visible light photocatalytic activity, J. Phys. Chem. 115 (2011) 20555–20564.

[15] H.F. Cheng, B.B. Huang, Y. Dai, X.Y. Qin, X.Y. Zhang, One-step synthesis of the nanostructured AgI/BiOI composites with highly enhanced visible-light photocatalytic performances, Langmuir 26 (2010) 6618–6624.

[16] Y.Y. Li, J.S. Wang, H.C. Yao, L.Y. Dang, Z.J. Li, Chemical etching preparation of $BiOI/Bi_2O_3$ heterostructures with enhanced photocatalytic activities, Catal. Commun. 12 (2011) 660–664.

[17] T.B. Li, G. Chen, C. Zhou, Z.Y. Shen, R.C. Jin, J.X. Sun, New photocatalyst BiOCl/BiOI composites with highly enhanced visible light photocatalytic performances, Dalton Trans. 40 (2011) 6751–6758.

[18] X. Xiao, R. Hao, M. Liang, X. Zuo, J. Nan, L. Li, W. Zhang, One-pot solvothermal synthesis of three-dimensional (3D) BiOI/BiOCl composites with enhanced visible-light photocatalytic activities for the degradation of bisphenol-A, J. Hazard. Mater. 233–234 (2012) 122–130.

[19] M.A. Gondal, X.F. Chang, M.A. Ali, Z.H. Yamani, Q. Zhou, G.B. Ji, Adsorption and degradation performance of Rhodamine B over BiOBr under monochromatic 532 nm pulsed laser exposure, Appl. Catal. A: Gen. 397 (2011) 192–200.

[20] J.M. Song, C.J. Mao, H.L. Niu, Y.H. Shen, S.Y. Zhang, Hierarchical structured bismuth oxychlorides: Self-assembly from nanoplates to nanoflowers via a solvothermal route and their photocatalytic properties, Cryst. Eng. Commun. 12 (2010) 3875–3881.

[21] D. Zhang, M. Wen, B. Jiang, G. Li, J. Yu, Ionothermal synthesis of hierarchical BiOBr microspheres for water treatment, J. Hazard. Mater. 211–212 (2012) 104–111.

[22] D. Sharma, A. Bansal, R. Ameta, H.S. Sharma Photocatalytic degradation of Azure B using bismuth oxide semiconducting powder, Chem. Technol. 3 (2011) 1008–1014.

[23] B. Chai, H. Zhou, F. Zhang, X. Liao, M. Ren, Visible light photocatalytic performance of hierarchical BiOBr microspheres synthesized via a reactable ionic liquid, Mater. Sci. Semicond. Process. 23 (2014) 151–158.

[24] X. Chang, J. Huang, C. Cheng, Q. Sui, W. Sha, G. Ji, S. Deng, G. Yu, BiOX (X = Cl, Br, I) photocatalysts prepared using $NaBiO_3$ as the Bi source: Characterization and catalytic performance, Catal. Commun. 11 (2010) 460–464.

[25] Y. Feng, L. Li, J. Li, J. Wang, Synthesis of mesoporous BiOBr 3D microspheres and their photodecomposition for toluene, J. Hazard. Mater. 192 (2011) 538–544.

[26] J. Xu, L. Li, C. Guo, Y. Zhang, S. Wang, Removal of benzotriazole from solution by BiOBr photocatalysis under simulated solar irradiation, Chem. Eng. J. 221 (2013) 230–237.

[27] C. Chang, L. Zhu, Y. Fu, X. Chu, Highly active Bi/BiOI composite synthesized by one-step reaction and its capacity to degrade bisphenol A under simulated solar light irradiation, Chem. Eng. J. 233 (2013) 305–314.

[28] L. Zhang, X.F. Cao, X.T. Chen, Z.L. Xue, BiOBr hierarchical microspheres: Microwave-assisted solvothermal synthesis, strong adsorption and excellent photocatalytic properties, J. Colloid Interface Sci. 354 (2011) 630–636.

[29] G. Li, F. Qin, H. Yang, Z. Lu, H. Sun, R. Chen, Facile microwave synthesis of 3D flowerlike BiOBr nanostructures and their excellent Cr(VI) removal capacity, J. Inorg. Chem. 25 (2012) 2508–2513.

[30] C. Yu, F. Cao, G. Li, R. Wei, J. Yu, R. Jin, Q. Fan, C. Wang, Novel noble metal (Rh, Pd, Pt)/BiOX(Cl, Br, I) composite photocatalysts with enhanced photocatalytic performance in dye degradation, J. Sep. Purif. Technol. 120 (2013) 110–122.

[31] C.L. Yu, C.F. Fan, X.J. Meng, K. Yang, F.F. Cao, X. Li, A novel Ag/BiOBr nanoplate catalyst with high photocatalytic activity in the decomposition of dyes, React. Kinet., Mech. Catal. 103 (2011) 141–151.

[32] C.L. Yu, F.F. Cao, Q. Shu, Y.L. Bao, Z.P. Xie, J.C. Yu, K. Yang, Characterization and photocatalytic performance of Ag/BiOX (X = Cl, Br, I) heterojunction photocatalysts, J. Acta Phys. Chim. Sin. 28 (2012) 647–653.

[33] S. Ge, K. Zhao, L. Zhang, Microstructure—dependent photoelectrochemical and photocatalytic properties of BiOI, J. Nanopart. Res. 14 (2012) 1015–1026.

[34] J. Cao, B. Xu, H. Lin, B. Luo, S. Chen, Chemical etching preparation of BiOI/BiOBr heterostructures with enhanced photocatalytic properties for organic dye removal, J. Chem. Eng. 185 (2011) 91–99.

[35] EPA method 508, Determination of chlorinated pesticides in water by gas chromatography with an electron capture detector, Rev. 3, 2007.

[36] EPA method 608, Organochlorine pesticides and PCBs by GC/HSD, Revision a, 2013.

[37] X. Shi, X. Chen, X. Chen, S. Zhou, S. Lou, Solvothermal synthesis of BiOI hierarchical spheres with homogeneous sizes and their high photocatalytic performance, J. Mater. Lett. 68 (2011) 296–299.

[38] Z. Jia, F. Wang, F. Xin, B. Zhang, Simple solvothermal routes to synthesize 3D $BiOBr_xI_{1-x}$ microspheres and their visible-light-induced photocatalytic properties, Ind. Eng. Chem. Res. 50 (2011) 6688–6694.

[39] J.W. Kramer, S.A. Isaacs, V. Manivannan, Microwave-assisted metathesis synthesis of Schoenfliesite-type $MSn(OH)_6$ (M = Mg, Ca, Zn, and Sr) materials, J. Mater. Sci. 44 (2009) 3387–3392.

[40] C.H. Chiou, R.S. Juang, Photocatalytic degradation of phenol in aqueous solutions by Pr-doped TiO_2 nanoparticles, J. Hazard. Mater. 149 (2007) 1–7.

[41] C. Suwanchawalit, S. Wongnawa, Influence of calcination on the microstructures and photocatalytic activity of potassium oxalate-doped TiO_2 powders, Appl. Catal. A: Gen. 338 (2008) 87–99.

[42] M. Behnajady, B. Alizade, N. Modirshahla, Synthesis of Mg-doped TiO_2 nanoparticles under different conditions and its photocatalytic activity, Photochem. Photobiol. 87 (2011) 1308–1314.

[43] C.C. Wong, W. Chu, The direct photolysis and photocatalytic degradation of alachlor at different TiO_2 and UV sources, Chemosphere 50 (2003) 981–987.

[44] R.S. Suri, J. Liu, D.W. Hand, J.C. Crittenden, D.L. Perram, M.E. Mullins, Heterogeneous photocatalytic oxidation of hazardous organic contaminants in water, Water Environ. Res. 65(1993) 665–673.

[45] O.K. Dalrymple, E. Stefanakos, M.A. Trotz, D.Y. Goswami, A review of the mechanisms and modeling of photocatalytic disinfection, Appl. Catal. B: Environ. 98 (2010) 27–38.

[46] H. Gupta, S. Tanaka, Photocatalytic mineralisation of perchloroethylene using titanium dioxide, Water Sci. Technol. 31 (1995) 47–54.

[47] N. Daneshvar, D. Salari, A.R. Khataee, Photocatalytic degradation of azo dye acid red 14 in water: Investigation of the effect of operational parameters, J. Photochem. Photobiol. A 157 (2003) 111–116.

[48] D. Jiang, H. Zhao, S. Zhang, R. John, G.D. Will, Photo-electrochemical measurement of phthalic acid adsorption on porous TiO_2 film electrodes, J. Photochem. Photobiol. A 156 (2003) 201–206.

[49] X. Zhao, Y. Wang, Z. Shi, C. Fan, Photocatalytic treatment of MO in water with BiOBr photocatalyst, Mater. Sci. Forum 694 (2011) 554–558.

[50] W. Ling-Li, M.W. Hong, W.S. Lian, Z. Yu, J.M. Ke, L.R. Ping, H.Y. Ping, The contrastive research in the photocatalytic activity of BiOBr synthesized by different reactants, Nanomaterials 2012 (2010) 1–9.

[51] W. Chu, W.K. Choy, T.Y. So, The effect of solution pH and peroxide in the TiO_2-induced photocatalysis of chlorinated aniline, J. Hazard. Mater. 141 (2007) 86–91.

[52] Y.N. Tan, C.L. Wong, A.R. Mohamed, An overview on the photocatalytic activity of Nano-doped-TiO_2 in the degradation of organic pollutants, ISRS Mater. Sci. (2011) 1–18.

[53] L. Andronic, A. Enesca, C. Vladuta, A. Duta, Photocatalytic activity of cadmium doped TiO_2 films for photocatalytic degradation of dyes, Chem. Eng. J. 152 (2009) 64–71.

[54] N.A. Jamalluddin, A.Z. Abdullah, Reactive dye degradation by combined Fe(III)/TiO_2 catalyst and ultrasonic irradiation: Effect of Fe(III) loading and calcination temperature, Ultrason. Sonochem. 18 (2011) 669–678.

[55] M.A. Behnajady, B. Alizade, N. Modirshahla, Synthesis of Mg-doped TiO_2 nanoparticles under different conditions and its photocatalytic activity, Photochem. Photobiol. 87 (2011) 1308–1314.

[56] J. Wang, Y. Yu, L. Zhang, Highly efficient photocatalytic removal of sodium pentachlorophenate with Bi_3O_4Br under visible light, Appl. Catal. B: Environ. 136–137 (2013) 112–121.

[57] J. Zhang, F.J. Shi, J. Lin, D.F. Chen, J.M. Gao, Z.X. Huang, X.X. Ding, C.C. Tang, Self-assembled 3-D architectures of BiOBr as a visible light-driven photocatalyst, Chem. Mater. 20 (2008) 2937–2941.

[58] L. Lin, M. Huang, L. Long, Z. Sun, W. Zheng, D. Chen, Fabrication of a three-dimensional BiOBr/BiOI photocatalyst with enhanced visible light photocatalytic performance, Ceram. Int. 40 (2014) 11493–11501.